Lateral Position Error Reduction Using Misalignment-Sensing Coils in Inductive Power Transfer Systems

Ivan Cortes and Won-jong Kim, *Senior Member, IEEE*

***Abstract*—Inductive power transfer (IPT) remains one of the most common ways to achieve wireless power transmission, operating on the same electromagnetic principle as electrical transformers but with an air core instead of an iron core. IPT has been implemented in many applications, including wireless charging of consumer products like smartphones and electric vehicles. However, one challenge with using IPT is ensuring precise alignment between the primary and secondary coils of the system so that maximum power transfer can take place. In this paper, the use of misalignment-sensing coils to detect and correct lateral misalignments in an IPT system is modeled and tested. The sensing coils exploit magnetic-field symmetry to give a nonlinear measurement of misalignment direction and magnitude. Experiments using such sensing coils give a misalignment sensing resolution better than 1 mm when applied to a commercial smartphone wireless charger. Voltage readings from the sensing coils are used for closed-loop control of an experimental two-dimensional coil positioner that can reduce lateral misalignments as large as 35 mm to less than 1.4 mm, allowing for effective power transfer. A similar sensing coil concept can be used to reduce lateral misalignments in scaled IPT systems, such as electric-vehicle wireless chargers.**

***Index Terms*—Electric sensing devices, magnetic sensors, motion detection, wireless power transmission.**

I. Introduction

MOBILE devices are increasingly in need of convenient and efficient ways to be powered. Wireless power transmission is of special interest because it eliminates the need for physical contact between a power source and an end device. Advantages of wireless power transmission include eliminating electrical contact wear, increasing device mobility, providing isolation from the environment, and reducing the battery capacity needed for operation [1].

Manuscript received June 1, 2017; revised November 9, 2017; accepted January 3, 2018. Date of publication February 2, 2018; date of current version April 16, 2018. This work was supported by the National Science Foundation under Award HRD-1502335 "Texas A&M University System Louis Stokes Alliance for Minority Participation (TAMUS LSAMP) Bridge to the Doctorate (BTD) Cohort XI (2015-2017) Program." Recommended by Technical Editor Z. Sun. *(Corresponding author: Ivan Cortes.)*

The authors are with the Department of Mechanical Engineering, Texas A&M University, College Station, TX 77843-3123 USA (e-mail: icorteso@tamu.edu; wjkim@tamu.edu).

Color versions of one or more of the figures in this paper are available online at http://ieeexplore.ieee.org.

Digital Object Identifier 10.1109/TMECH.2018.2801250

Inductive power transfer (IPT) is the most common method of wireless power transmission. As its name suggests, IPT makes use of the inductive link between coils in proximity of each other to transfer energy [2]. Tesla is widely regarded as a pioneer of IPT since he experimented with powering electrical devices through the air in the late 1800s [3]. Decades before, electromagnetic induction had been discovered by Faraday and Henry, and in 1885 Stanley created the first practical electrical transformer—a prime example of IPT [4], [5]. IPT has been implemented in the wireless charging of devices like mobile phones, electric vehicles, medical implants, and others [1], [6].

In an electrical transformer, inductive coils are closely coupled with each other using an iron core, allowing power-transfer efficiencies easily greater than 95%. In IPT for wireless charging, the power-source and end-device coils are coupled loosely through an air core. Device mobility provides a challenge for IPT wireless charging systems since coil misalignments weaken the inductive link and result in decreased power transfer [7]–[9].

In the literature, IPT misalignment intolerance has been addressed in at least the three following ways:

1) improving coil circuits using resonance tuning;
2) altering the number, geometry, or orientation of coils;
3) detecting and correcting misalignments between the coils.

In resonance-based tuning compensation circuits with series or parallel capacitors are added so that the resonance frequency between the transmitting and receiving coils is matched [10]. In some cases, such as in the widely-adopted Qi wireless charging standard, the operating frequency or the power level of the charger is modulated in real time using closed-loop control [11], [12]. Resonance-based tuning increases the IPT transmission range and can be used to reduce the magnetic field effects on foreign objects.

Introducing additional IPT coils or changing their geometry has also been used to address misalignment intolerance. For example, the power source may be connected to an array of transmitting coils rather than just one, effectively increasing the magnetic flux density distribution [13]. A similar concept was used for rodent tracking within a cage in [14]. In another study, orthogonal receiving coils were used to increase power transfer when there were angular misalignments [15].

A third way to address misalignment intolerance is to detect misalignments and correct them. In many commercial products, visual markers or light indicators assist users in aligning their device with the IPT transmitter. In more sophisticated systems,

1083-4435 © 2018 IEEE. Personal use is permitted, but republication/redistribution requires IEEE permission.
See http://www.ieee.org/publications_standards/publications/rights/index.html for more information.

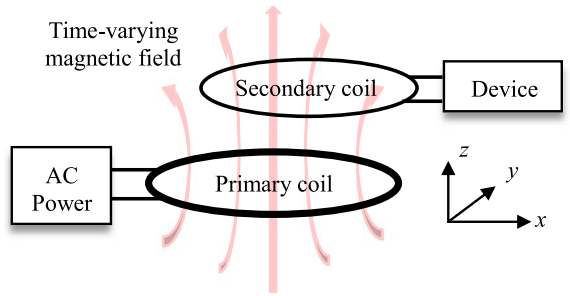

Fig. 1. Basic setup for an IPT system. The key working principle is an induced voltage in the secondary coil as a result of the time-varying magnetic flux produced by the primary coil.

misalignments are detected using various sensors [16]. The Qi standard provides some suggestions for misalignment detection, including the use of capacitive, resistive, or inductive sensing grids [8]. Detecting misalignments introduces the possibility of automatically correcting them in real time. For example, one research group used sensing coils to detect misalignments between a vehicle and an in-road wireless charger as it moved [17]. In [18] and [19], auxiliary coils are added to an IPT system to sense lateral misalignments.

In this paper, the use of sensing coils for misalignment detection in an IPT system is modeled and tested. The focus is on the lateral misalignment between two IPT coils that remain parallel to each other and at a fixed distance—a scenario consistent with applications such as wireless charging of electric vehicles, home appliances, and other mobile devices. Successful misalignment detection using the sensing coils allows for experimentation with closed-loop control of a two-dimensional (2-D) coil positioner—a variation of which can be implemented in charging applications to ensure the maximum power transfer takes place. Automatic alignment for IPT is especially suited for autonomous charging applications that have recently generated interest [20], [21].

This paper consists of seven sections. In Section II, the basic working principle of an IPT system is reviewed and analyzed considering a circular coil geometry. Section III introduces the sensing coils proposed for detecting lateral misalignments in the IPT system. This section presents simulated results of the sensing coil's signal output. An experimental setup that consists of a sensing coil assembly and a 2-D positioner is described in Section IV. In Section V, a closed-loop controller for automatic alignment using the 2-D positioner is presented. The results of three sensing-coil experiments are given in Section VI. The experiments measure the sensing coils' voltage outputs at various misalignment conditions and the 1-D and 2-D automatic alignment performances of the alignment system. Section VII presents the conclusions from these experiments.

II. IPT Analysis

A simple model of an IPT system is developed here using electromagnetic principles. In a basic IPT system (see Fig. 1), there is one primary coil connected to an ac power source and a secondary coil connected to the end device. The time-varying magnetic flux density created by the current-carrying primary coil can be calculated using the Biot–Savart law, and the

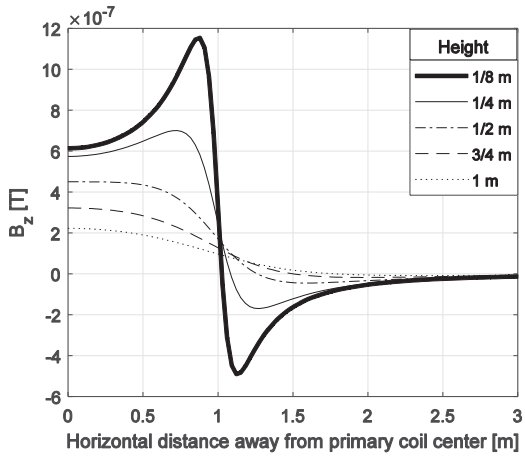

Fig. 2. Magnetic flux density's z component as a function of the horizontal distance away from the primary coil center at various heights of 1/8, 1/4, 1/2, 3/4, and 1 m. Results shown are for a circular primary coil of 1 m with 1-A current. The magnitude of B_z is greatest directly above the primary coil.

induced voltage in the secondary coil can be calculated using Faraday's law of magnetic induction. Most importantly, it is the time derivative of the magnetic flux penetrating the secondary coil that induces a voltage in the secondary coil. Assuming a sinusoidal ac power source, the induced voltage in the secondary coil can be expressed in the following form:

$$v_{induced} = \left(n\,\omega \oint B_z\, da \right) \sin(\omega t) \tag{1}$$

where

n: number of turns in the secondary coil;
ω: operating frequency of the ac power source [rad/s];
B_z: magnetic flux density z component [T];
da: infinitesimal coil area element [m^2].

Equation (1) predicts many of the known characteristics of IPT systems. For example, increasing the operating frequency or the number of secondary coil turns generally increases the power transfer. Furthermore, to maximize power transfer to a secondary coil, the magnetic flux density penetrating it should be maximized. The misalignment intolerance of IPT systems is a result of the spatially-dependent magnetic-flux-density distribution since misalignments tend to reduce the magnetic flux penetrating the secondary coil. In (1), the effects of coil movement are ignored since the time-varying flux contribution from coil movement is expected to be insignificant compared to that due to the high-frequency alternating field.

A. Magnetic-Flux-Density Distribution

The spatial distribution of the magnetic flux density is a key to understanding misalignment effects on IPT. For a circular primary coil, which is a common geometry in IPT systems, the magnetic flux density is axisymmetric. Fig. 2 shows the radial and z dependence of B_z due to a normalized primary coil of 1-m radius and 1-A current. The greatest magnitudes of B_z occur above the primary coil, and greater heights have a lower B_z everywhere. At low heights (relative to the primary coil radius, such as 1/8 m in Fig. 2), the magnetic flux density initially

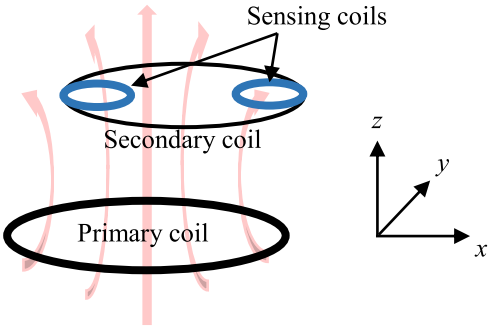

Fig. 3. Proposed sensing coils attached symmetrically to the secondary coil. As the secondary coil moves in the x-direction, the sensing coils can be used to measure imbalances in the magnetic flux density around the secondary coil.

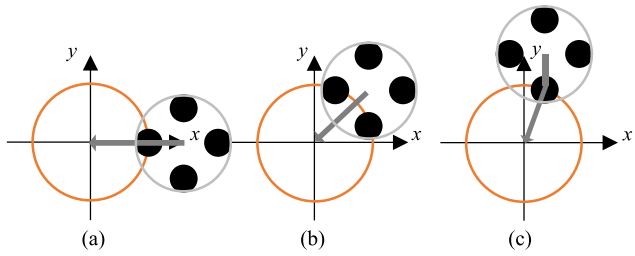

Fig. 4. Scenarios of lateral misalignment that can be detected by the sensing coils. The circle centered at the origin represents the area in which the sensing coils must remain to experience an induced voltage and is estimated to be approximately the size of the primary coil. The circle around the sensing coils represents the secondary coil, which moves with the sensing coils.

increases with horizontal distance. This is because these locations are near the primary coil wire, where the magnetic flux density is largest. The flux density at each location in space is contributed by each infinitesimal wire segment with a magnitude proportional to the inverse square of the distance to the respective segment.

According to Fig. 2, a secondary coil parallel to the primary coil should remain concentric and close to the primary coil for appreciable power transfer to occur. This is because the flux penetrating the secondary coil is a surface integration of B_z over the secondary coil area. If the secondary coil is near the same size as the primary coil then even small lateral misalignments reduce the magnetic flux penetrating the secondary coil and power transfer is reduced. Numerous studies have shown how misalignments affect power transfer efficiency [6], [7].

To detect lateral misalignments in an IPT system, one might monitor the magnetic flux density within the secondary coil. According to (1), the induced voltage can serve as a measurement of magnetic flux. However, the induced voltage in the secondary coil can change due to the factors other than misalignment, and alternative ways to detect misalignments have been researched [16]. Furthermore, it may be difficult to determine the misalignment direction from the induced voltage in the secondary coil alone.

III. Misalignment-Sensing Coils

Rather than monitoring the induced voltage of the secondary coil to detect IPT misalignments, dedicated misalignment-sensing coils are introduced.

A. Operating Principle

The use of sensing coils is based on the observations made in Fig. 2—that the flux-density distribution is axisymmetric and that B_z is largest above the primary coil. Two small coils are attached symmetrically to the secondary coil and move along with it as shown in Fig. 3. When there is no lateral misalignment, the left and right sensing coils experience the same induced voltage due to the symmetric flux-density distribution from the primary coil. However, as the secondary coil moves in the x-direction, different induced voltages occur in the left and right sensing coils. The difference in induced voltages can be used to detect the x misalignment. Magnetic flux from the secondary coil affects both sensing coils equally, so it does not affect the voltage difference at any time. The placement and size of the sensing coils will determine the range of misalignment amounts that can be detected. Due to the distribution shown in Fig. 2, it is predicted that the sensing coils will experience induced voltages as long as they remain above the primary coil, where the flux density is largest.

The sensing-coil configuration in Fig. 3 can be used to detect x-direction misalignments, but additional sensing coils can be introduced to sense misalignments in any radial direction away from the z-axis. In this paper, the simple case where two sensing coils are added for the x-direction and two for the y-direction is considered. Misalignment detection and correction in these two orthogonal directions allows for positioning in an xy plane that is parallel to the primary coil. Misalignments in this plane are referred to as lateral misalignments. Sensing and correcting lateral misalignments is accomplished in this paper by treating the x- and y-directions separately using closed-loop control.

To predict the effects of independent x- and y-direction misalignment reduction using closed-loop control, consider the three cases presented in Fig. 4. These scenarios represent three different types of lateral misalignment that can occur and the expected outcomes for corrective action using the sensing coils with independent x and y control loops. The black circles are the sensing coils and the circle centered at the origin represents the region in which the sensing coils experience an induced voltage. Recall that the size of this circle is expected to be approximately the size of the primary coil. The arrow pointing to the origin represents a plausible trajectory for alignment. In scenario (a) the misalignment is in the x-direction only and the largest misalignment distance that can be detected is about one primary coil diameter. In scenario (b) the misalignment is equal in both the x- and y-directions, and the maximum misalignment that can be detected is less than the primary coil diameter. In (a) only the x controller is needed for alignment, and in (b) the x and y controllers can work simultaneously to provide a trajectory to alignment. In scenario (c) the misalignment is 2-D but greater in the y-direction than the x-direction, such that only the bottom y sensing coil remains within the maximum detection region. In this case, the x-direction misalignment cannot be detected initially because neither of the x sensing coils are within the detection region. However, as the y-direction misalignment is being corrected, the x sensing coils will enter the detection region and the x-direction misalignment will eventually be

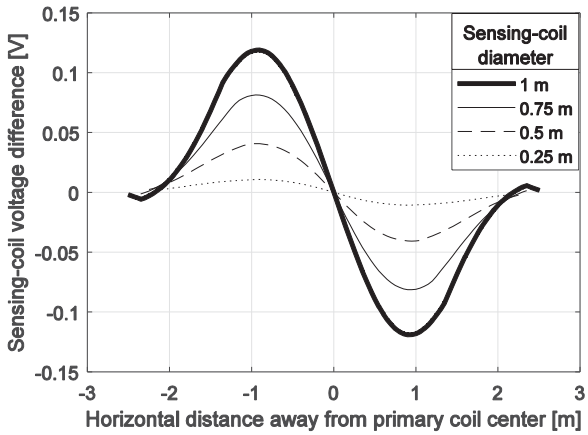

Fig. 5. Simulated voltage difference between sensing coils as they move horizontally away from the primary coil center. Results for various sensing-coil diameters are included. The primary coil has a 1-m radius and carries 1 A of current. The sensing coils are at 1-m height and are spaced so that they fit inside a 1-m radius circle. The voltage sign indicates misalignment direction.

corrected. In such a scenario, the trajectory to alignment will not be straight.

The scenarios illustrated in Fig. 4 suggest that the arrangement of four sensing coils and independent control loops in the x- and y-directions can be used to provide automatic IPT alignment for various lateral misalignments within a limited range. The smallest range occurs in scenario (b), where the misalignment is equal in both the x- and y-directions, and the largest range occurs in scenario (a), where the misalignment is only in one direction. The difference in these ranges depends on the coil geometries. A trigonometric estimate is that the range in (b) will be less than 70% of that in (a). Another anticipated consequence of using separate x- and y-direction control is nonstraight trajectories to alignment in some cases. Different alignment speeds in each direction would also cause nonstraight alignment trajectories.

B. Simulation Results

Using a finite-element approximation of Faraday's law, the induced voltage for sensing coils such as those in Fig. 3 was simulated. Fig. 5 shows the simulation results as two sensing coils of various diameters are moved along the x-direction. For each plotted curve, the sensing coils are at 1-m height and are spaced so that they fit just inside a circle of 1-m radius. According to Fig. 2, this spacing ensures that both sensing coils are within the strong magnetic-flux-density region when there is no misalignment and that one of the sensing coils experiences a decrease in flux when there is misalignment. As proposed, it is the voltage difference between the left and right sensing coils that is plotted. The results show that the voltage difference can be used to detect misalignment direction, but it is more difficult to tell the misalignment magnitude due to the nonlinear trend.

The results of Fig. 5 also support the prediction that the maximum misalignment distance that can be detected in the 1-D case is about one primary coil diameter (2 m in the simulation). This appears to be true regardless of the sensing-coil diameter although larger diameters give larger voltages. According to (1), increasing the number of sensing-coil turns will also increase the induced voltage.

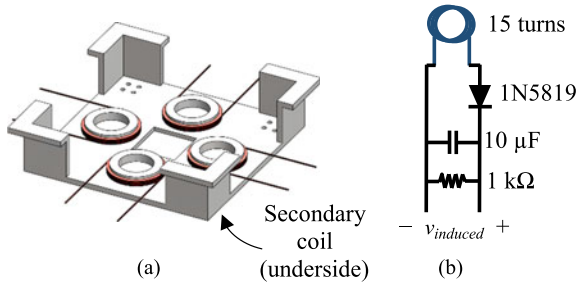

Fig. 6. (a) Custom sensing-coil fixture and (b) the rectifier circuit for dc measurement of the induced voltage amplitude. The 15-turn sensing coils are used to measure the magnetic flux around the secondary coil.

IV. Experimental Hardware

An experimental IPT setup using a sensing-coil assembly and commercial Qi wireless charger rated at 5 W was used to support the simulation results and to test automatic IPT lateral positioning using closed-loop control.

A. Sensing Coil Assembly

The sensing-coil fixture depicted in Fig. 6 was 3-D-printed to provide the sensing coil arrangement previously described, with two sensing coils for the x-direction and two for the y-direction. The secondary coil is fixed beneath the coil assembly—2 mm under the sensing coils. The diameter of each sensing coil is 12.7 mm (0.5 in) with 15 turns of AWG 25 wire. The sensing coils are spaced so that they fit just inside a circle with diameter equal to the primary coil diameter of 43 mm (1.7 in). The sensing-coil fixture geometry allows it to be attached to the rest of the sensing coil assembly of the positioner, which is presented in the next section.

A diode rectifier circuit with a smoothing capacitor and a shunt resistor was added to each sensing coil so that the induced voltage amplitude can easily be measured in dc form using an Arduino UNO board. The Arduino contains a 10-bit analog-to-digital converter with the input voltage swing between 0 and 5 V, giving a sensing resolution of about 4.9 mV. The rectifier circuits introduce power loss to the sensing coils. The power loss can be reduced by increasing the shunt resistor value. Furthermore, the sensing-coil circuits could be disconnected after alignment is completed so that they no longer affect the IPT system in any way.

B. Two-Dimensional Positioner

The sensing-coil fixture position above the Qi wireless charger is controlled by the experimental 2-D positioner assembly shown in Fig. 7. In this setup, the Qi charger remains stationary, and two stepper motors move the sensing coil fixture in the x- and y-directions at a constant height of 6 mm above the charger. The secondary coil remains 4 mm above the wireless charger—well within the charger's advertised working distance of 8 mm. The sensing-coil assembly holds the sensing-coil fixture and has linear ball bearings for smooth movement along the guide rails. The 2-D positioner allows for precise lateral

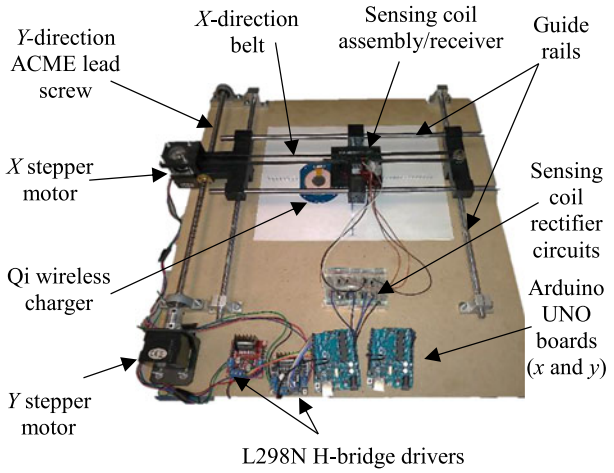

Fig. 7. Two-dimensional positioner used to create IPT lateral misalignments in the x- and y-directions. This system is also used to test automatic closed-loop alignment for the sensing coils with the wireless Qi charger.

misalignments to be introduced and for testing of closed-loop IPT alignment.

Each stepper motor in the positioner assembly provides 200 steps per revolution and is powered by an L298N H-bridge driver, which is commanded by an Arduino UNO board. The x-direction stepper motor is connected to the sensing coil assembly via a nonelastic belt and pulley, providing an x-positioning resolution of 0.2 mm per motor step. The y-direction stepper motor turns a leadscrew that moves the sensing coil assembly with a y-positioning resolution of 0.05 mm per motor step.

Using these stepper motors greatly simplifies the positioner dynamics. The permanent-magnet bipolar stepper motors provide movement in well-defined incremental steps that can be modeled as damped step responses with zero steady-state error. At each step, the inertia and friction of the positioner is overcome by the motor torque to provide a new equilibrium position. This "locked-step" mode of stepper motor operation allows the positioner to instantly start, stop, and even reverse direction at high speeds. The overall positioner movement can be modeled as a series of step responses with a finite response time per step. The overall speed of the positioner is determined by the time delay between subsequent motor steps.

V. Automatic Alignment Controller

To test the positioning system of Fig. 7, a closed-loop controller was developed. In this controller, the x- and y-direction loops are closed independently, with the sensing coils providing a measurement of misalignment in each direction. Due to the positioner dynamics, a simple proportional control law is used, where the speed of the positioner stepper motors is proportional to the sensing coil voltage magnitude. To ensure that the positioner remains in locked-step mode, one of the performance goals of control is to ensure that the motor speeds remain within an experimentally determined limit (about 250 r/min for the motors in Fig. 7). This speed allows sufficient time for each motor step to take place. Other goals are to reduce the misalignment in a reasonable time (on the order of seconds) and to minimize the 2-D trajectory to alignment.

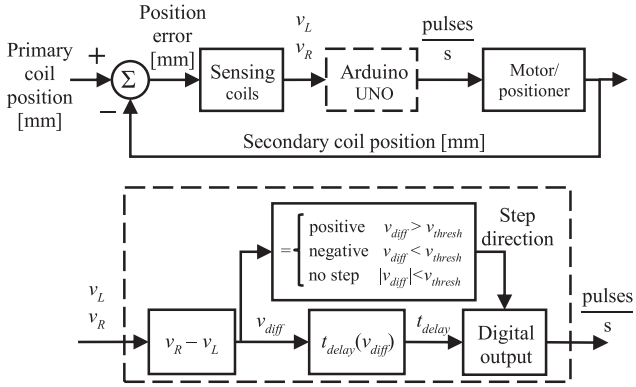

Fig. 8. Closed-loop control for automatic positioning of the secondary coil above the primary coil using sensing coils to detect misalignments.

Due to the anticipated nonlinear voltage trend of Fig. 5, proportional control means that the highest motor speed occurs when the misalignment amount is about half of the primary coil diameter. The slowest speed occurs as the positioner nears alignment. Gradually stopping makes it less likely for the motor to be pulled off the locked-step mode from suddenly stopping. The movement direction is determined by the sign of the sensing coil voltage. The voltage difference is approximately 0 V when the system reaches alignment.

The proportional control structure, which is implemented separately for the x- and y-directions, is illustrated in Fig. 8. The functions of the Arduino are clearly labeled. First, the Arduino measures the voltages from the sensing coils and computes their difference. The motor step direction is determined from the sign of the voltage difference. Voltages that fall within a small deadband, set by the threshold voltage v_{thresh}, result in no motor movement. The threshold voltage was set at 0.05 V by experimentation to avoid the positioner's limit cycling when the voltage is nearly zero. Finally, the Arduino uses digital output to command the stepper motor at the appropriate step frequency. The time delay between steps determines the motor speed and is calculated using the linear equation

$$t_{delay}(v_{diff}) = t_{d,\,\max}\left(1 - |v_{diff}|\,/v_{\max}\right) \tag{2}$$

where

t_{delay}: time delay [ms];
$t_{d,\max}$: maximum time delay [ms];
v_{diff}: voltage difference between sensing coils [V];
$v_{\max}$: maximum voltage difference [V].

The time delay gets smaller as v_{diff} approaches $v_{\max}$, resulting in a faster motor speed. The value used for $v_{\max}$ in the forthcoming experiments was 0.75 V and was based on the results presented in Section VI. The $t_{d,\max}$ value used was 50 ms to set the slowest stepper motor speed. Slower speeds are achievable but increase the total response time.

If t_{delay} is too small, there is not enough time to complete each motor step and the motor is pulled off the locked-step mode. To avoid this, the t_{delay} value is not allowed to fall below an experimentally determined value. The minimum value was set at 1.33 ms (for a speed of 200 r/min) for the y stepper motor and 5.33 ms (50 r/min) for the x stepper motor. The y motor is allowed to move four times as fast as the x motor since the positioner distance traveled per step in the y-direction is four

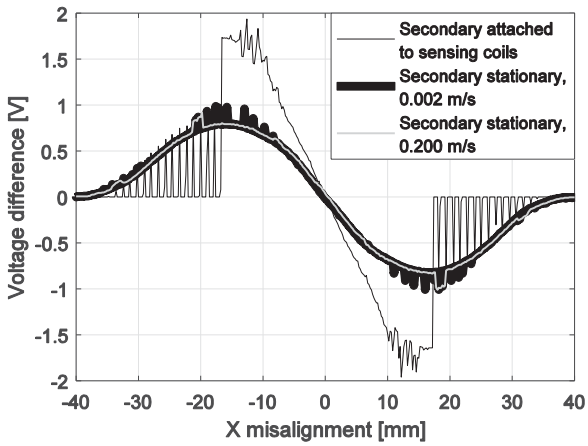

Fig. 9. Sensing-coil voltage difference measurements versus x-direction misalignment at various conditions. If the receiver moves with the sensing coils, the Qi charger increases its output and eventually enters a pulsating mode because the receiver moves out of range. The speed of the movement does not affect the voltage measurements.

times smaller than that of the x-direction. Limiting the speeds in this way is expected to result in straighter alignment trajectories since this does not allow the movement in the x-direction to be much faster than the y-direction.

VI. Experimental Results

A. Sensing-Coil Voltage Measurements

In the first experiment, the sensing coils are displaced from the aligned position above the Qi wireless charger, and their voltages are recorded. This procedure reproduces the simulation result presented in Fig. 5. The results of this experiment are shown in Fig. 9, where the voltage difference between the x sensing coils is plotted as a function of x-direction misalignment. Three distinct experimental conditions are plotted to show the effects of the secondary coil placement and of the movement.

In the first condition, the secondary coil moves with the sensing coils, as proposed for normal operation. The voltage magnitude initially increases linearly with misalignment. In this region, the Qi charger increases its power output to compensate for reduced power transfer due to misalignment. Beyond the misalignment of about ± 17 mm, the secondary coil is out of range, and the Qi charger enters a pulsating mode (a common behavior in commercial chargers). The sensing coils continue to detect the misalignment at each pulse up to about ± 38 mm.

The second condition plotted in Fig. 9 shows what the voltage trend looks like when the Qi charger operation is steady. To enforce this condition, the secondary coil is held stationary. That is, it does not move with the sensing coils. In this case, the voltage trend is similar to that in the simulation. This gives an idea of the sensing coil operation in a general IPT system with a steady primary coil power. The maximum misalignment detection range remains about 38 mm, which is near the primary coil diameter of 43 mm, as predicted in Fig. 5. Furthermore, the voltage sign indicates the misalignment direction, and the voltage difference is nearly zero when there is no misalignment. Comparing this result with the first plotted condition, one can see that the moving secondary coil alters the operation mode of

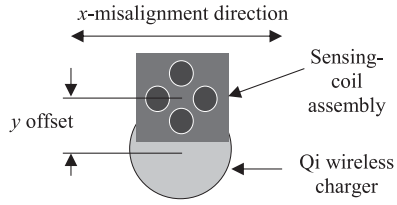

Fig. 10. Sensing-coil voltage measurements versus misalignment were repeated with added offsets in the orthogonal direction. This procedure tests the sensing coil performance for two-dimensional misalignments.

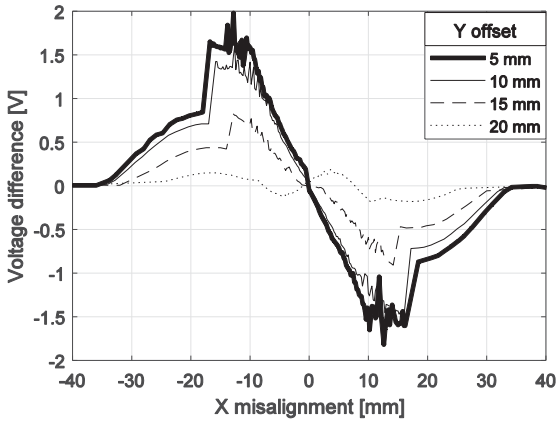

Fig. 11. Sensing-coil voltage measurements versus x-direction misalignment. Various offsets in the y-direction (orthogonal to x) are plotted.

the Qi charger, but it does not affect the operation principle of the sensing coils.

Finally, the third plotted condition in Fig. 9 shows that increasing the movement speed does not affect the sensing-coil voltage difference results significantly. This was predicted in the voltage expression (1), where velocity does not appear.

To investigate the effect of 2-D misalignments on the sensing coil performance, the voltage measurements were repeated with added offsets in the y-direction, as indicated in Fig. 10. These results are plotted in Fig. 11. For clarity, the pulsating region of the charger is replaced by smooth curves. As the y offset increases, the voltage magnitudes and the largest detectable misalignment distance decrease. At the largest misalignment (20 mm, which is about the radius of the primary coil in the Qi charger), the trend is no longer useful for determining misalignment direction since there are narrow positive and negative voltage regions for both directions of misalignment. At this large y offset, the x sensing coils barely pass through the area above the Qi charger coils.

The results of Figs. 9 and 11 can largely be summarized by concluding that to sense misalignments at least one of the sensing coils should be within the region above the primary coil. This prediction was also made from the simulation results.

B. One-Dimensional Automatic Alignment

With the functionality of the sensing coils confirmed, automatic positioning of the experimental IPT system was tested. This was accomplished using the proportional controller of Section V and the 2-D positioner presented in Fig. 7.

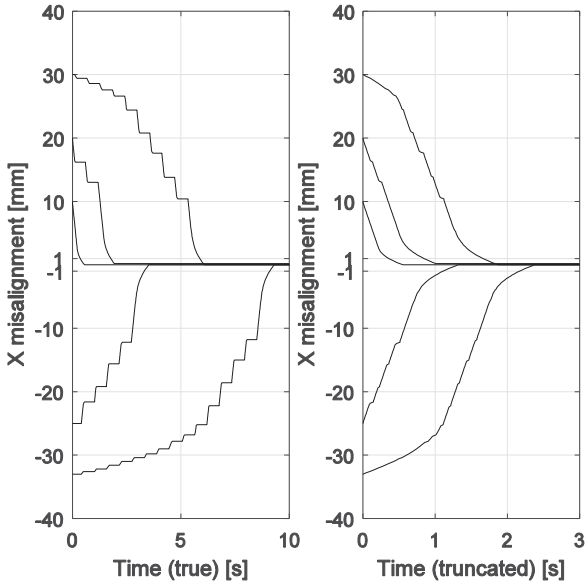

Fig. 12. Time responses for the positioner system given various initial misalignments in the x-direction. The system reduces misalignments to less than 1 mm in each case. The truncated time plot removes the time intervals of no movement that occur when the Qi charger is in pulsating mode.

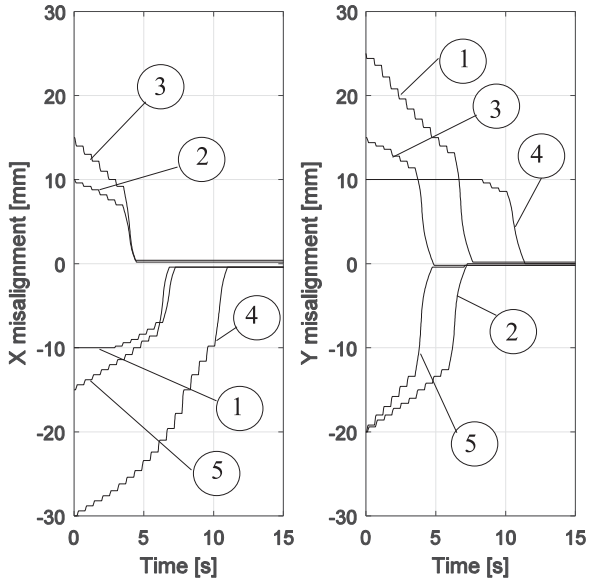

Fig. 13. Time responses for the positioner system given various initial misalignments in the x- and y-directions. The system reduces misalignments to less than 1 mm in each direction. Labels indicate the trial numbers.

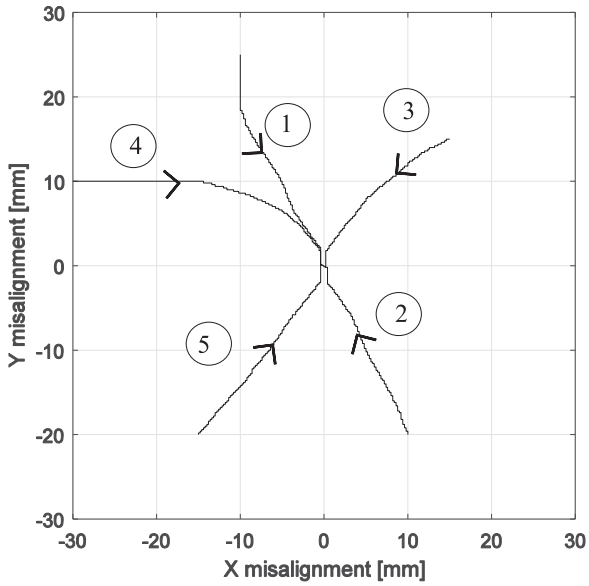

Fig. 14. Plotted trajectories in the xy plane for the 2-D automatic alignment trials. The trajectories are not always direct, but the misalignment is reduced to less than 1 mm in each of the x- and y-directions. Labels indicate the trial numbers.

The time responses for various initial misalignments in the x-direction are plotted in Fig. 12. In each trial, the positioner reduces the misalignment to less than 1 mm. The effect of the nonlinear sensing-coil voltage output can be seen in the varying motor speed throughout the response; the slowest motor speeds occur at large and small misalignment positions. In addition, the pulsating mode of the Qi charger, as described in Fig. 9, causes the positioner to move intermittently until the misalignment is less than about 10 mm. The time delay between the Qi charger pulses adds considerably to the total response time. To show what the response would be like without these pulse delays, the right plot in Fig. 12 shows the same responses with the time intervals of no movement truncated.

Near a 35-mm initial x-misalignment (not shown), control action failed since this position caused the sensing coils to fall outside of the maximum sensing range. From Fig. 9, it is evident that the farthest misalignment that can be detected is near 35 mm. Larger misalignments leave all of the sensing coils outside of the maximum sensing region.

C. Two-Dimensional Automatic Alignment

The automatic alignment response was also tested when the initial misalignment was 2-D. For this experiment, the sensing coil assembly was displaced to a certain location in the xy plane in the beginning. The system responses for various initial misalignments are plotted in Fig. 13. The same trials are plotted in Fig. 14 to show the positioner trajectories in the xy plane. For all trials, the final position error is less than 1 mm in each of the x- and y-directions, still with little overshoot. Thus, the total final position error is less than 1.4 mm. The nonstraight alignment paths result from different motor speeds in the x- and y-direction control loops. Scenario (c) of Fig. 4 occurs in trials 1 and 4 and also results in a nonstraight path to alignment. Nevertheless, the response times in Fig. 13 are similar to the 1-D experiments of Fig. 12.

Two-dimensional automatic positioning failed when the initial misalignment was 20 mm or greater in both the x- and y-directions. Thus, the maximum misalignment distance that can be detected in this scenario is about half of the Qi primary coil diameter. A 2-D misalignment that is equal in both the x- and y-directions represents the worst-case scenario for the four-sensing-coil configuration, since this type of motion allows for the least movement before all of the sensing coils go outside of the area above the primary coil.

VII. Conclusion

The use of dedicated misalignment-sensing coils for lateral misalignment detection in IPT systems was analyzed and tested in this paper. The focus was on IPT systems with a circular coil geometry that produce an axisymmetric magnetic field. The proposed sensing-coil assembly, which consists of four small coils and rectifier circuits, is attached to the IPT secondary coil and gives a measurement of the magnetic flux density differences in two orthogonal directions of the secondary coil. Differences in the sensing-coil voltages indicate a misalignment.

When tested on a Qi wireless charger and experimental 2-D positioning system, the proposed sensing coils gave a misalignment-sensing resolution better than 1 mm. The experimental results also suggest that the maximum misalignment amount that can be detected is near one primary-coil diameter. The nonlinear sensing-coil voltage output is easily used to detect the misalignment direction, but it is more difficult to determine the misalignment magnitude. Nevertheless, the sensing coil signals were successfully incorporated for the closed-loop proportional control of the experimental IPT system to reduce lateral misalignments to less than 1.4 mm, allowing for effective power transmission.

The misalignment-sensing coils presented in this paper provide a contactless and nonintrusive way to detect lateral misalignments in a commercial wireless charging IPT system. This lateral misalignment detection and correction method is promising to increase the effectiveness of similar IPT systems that may also be vulnerable to lateral misalignments, such as those used in electric-vehicle wireless charging.

References

[1] I. Mayordomo, T. Dräger, P. Spies, J. Bernhard, and A. Pflaum, "An overview of technical challenges and advances of inductive wireless power transmission," *Proc. IEEE*, vol. 101, no. 6, pp. 1302–1311, Jun. 2013.

[2] G. Covic and J. Boys, "Inductive power transfer," *Proc. IEEE*, vol. 101, no. 6, pp. 1276–1289, Jun. 2013.

[3] N. Tesla, "Apparatus for transmission of electrical energy," U.S. Patent 649621, May 15, 1900.

[4] F. T. Ulaby and U. Ravaioli, "Maxwell's equations for time-varying fields," in *Fundamentals of Applied Electromagnetics*, 7th ed. Upper Saddle River, NJ, USA: Pearson, 2015, ch. 6, sec. 1, pp. 282–283.

[5] W. Stanley, "Alternating-current development in America," *J. Franklin Inst.*, vol. 173, no. 6, pp. 561–580, Jun. 1912.

[6] J. Gao, G. Yan, Z. Wang, S. He, F. Xu, P. Jiang, and D. Liu, "Design and testing of a motor-based capsule robot powered by wireless power transmission," *IEEE/ASME Trans. Mechatronics*, vol. 21, no. 2, pp. 683–693, Apr. 2016.

[7] Y. Gao, A. Ginart, K. B. Farley, and Z. T. H. Tse, "Misalignment effect on efficiency of wireless power transfer for electric vehicles," in *Proc. IEEE Appl. Power Electron. Conf. Expo.*, Mar. 2016, pp. 3526–3528.

[8] R. W. Carlson and B. Normann, "Test results of the PLUGLESS inductive charging system from Evatran Group, Inc.," *SAE Int. J. Alternative Powertrains*, vol. 3, no. 1, pp. 64–71, May 2014.

[9] Z. Zhang and K. T. Chau, "Homogenous wireless power transfer for move-and-charge," *IEEE Trans. Power Electron.*, vol. 30, no. 11, pp. 6213–6220, Nov. 2015.

[10] Z. Dang, Y. Cao, and J. A. A. Qahouq, "Reconfigurable magnetic resonance-coupled wireless power transfer system," *IEEE Trans. Power Electron.*, vol. 30, no. 11, pp. 6057–6069, Nov. 2015.

[11] Wireless Power Consortium. Get the Specs on Qi, Nov. 30, 2016. [Online] Available: https://www.wirelesspowerconsortium.com/developers/specification.html

[12] S. Y. Hui, "Planar wireless charging technology for portable electronic products and Qi," *Proc. IEEE*, vol. 10, no. 6, pp. 1290–1301, Jun. 2013.

[13] S. A. Mirbozorgi, H. Bahrami, M. Sawan, and B. Gosselin, "A smart multicoil inductively coupled array for wireless power transmission," *IEEE Trans. Ind. Electron.*, vol. 61, no. 11, pp. 6061–6070, Nov. 2014.

[14] S. A. Mirbozorgi, H. Bahrami, M. Sawan, and B. Gosselin, "A smart cage with uniform wireless power distribution in 3D for enabling long-term experiments with freely moving animals," *IEEE Trans. Biomed. Circuits Syst.*, vol. 10, no. 2, pp. 424–434, Apr. 2016.

[15] J. P. W. Chow, N. Chen, H. S. H. Chung, and L. L. H. Chan, "An investigation into the use of orthogonal winding in loosely coupled link for improving power transfer efficiency under coil misalignment," *IEEE Trans. Power Electron.*, vol. 30, no. 10, pp. 5632–5649, Oct. 2015.

[16] Y. Gao, A. A. Oliveira, K. B. Farley, and Z. T. H. Tse, "Magnetic alignment using existing charging facility in wireless EV chargers," *J. Sens.*, vol. 2016, Dec. 2015, Art. no. 5670510.

[17] K. Hwang *et al.*, "Autonomous coil alignment system using fuzzy steering control for electric vehicles with dynamic wireless charging," *Math. Probl. Eng.*, vol. 2015, Nov. 2015, Art. no. 205285.

[18] K. Hwang *et al.*, "An autonomous coil alignment system for the dynamic wireless charging of electric vehicles to minimize lateral misalignment," *Energies*, vol. 10, no. 3, pp. 1–20, Mar. 2017.

[19] Y. Gao, C. Duan, A. A. Oliveira, A. Ginart, K. B. Farley, and Z. T. H. Tse, "Three-dimensional coil positioning based on magnetic sensing for wireless EV charging," *IEEE Trans. Transp. Electrification*, vol. 3, no. 3, pp. 578–588, Sep. 2017. [Online]. Available: http://ieeexplore.ieee.org/document/7907313/

[20] P. Phamduy, J. Cheong, and M. Porfiri, "An autonomous charging system for a robotic fish," *IEEE/ASME Trans. Mechatronics*, vol. 21, no. 6, pp. 2953–2963, Dec. 2016.

[21] X. Li, Z. Sun, D. Cao, Z. He, and Q. Zhu, "Real-time trajectory planning for autonomous urban driving: Framework, algorithms, and verifications," *IEEE/ASME Trans. Mechatronics*, vol. 21, no. 2, pp. 740–753, Apr. 2016.

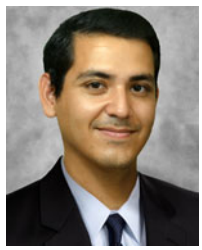

Ivan Cortes received the B.S. and M.S. degrees in mechanical engineering from Texas A&M University (TAMU), College Station, TX, USA, in 2015 and 2017, respectively. He is currently working toward the Ph.D. degree in mechanical engineering at TAMU.

During his undergraduate studies, he worked as a Technician with the TAMU Turbomachinery Laboratory, assisting in research of pump seal rotordynamics. He later held the position of Etch Equipment Engineer with Freescale Semiconductor. His research interests include the design and control of mechatronic systems, novel sensors, and actuators.

Mr. Cortes is a Fellow of the NSF-funded Texas A&M University System Louis Stokes Alliance for Minority Participation (TAMUS LSAMP) Bridge to the Doctorate (BTD) Program Cohort XI.

Won-jong Kim (S'89–M'97–SM'03) received the B.S. (*summa cum laude*) and M.S. degrees in control and instrumentation engineering from Seoul National University, Seoul, South Korea, in 1989 and 1991, respectively, and the Ph.D. degree in electrical engineering and computer science from the Massachusetts Institute of Technology (MIT), Cambridge, MA, USA, in 1997.

Since 2000, he has been with the Department of Mechanical Engineering, Texas A&M University (TAMU), College Station, TX, USA, where currently he is an Associate Professor and was the inaugural Holder of the Dietz Career Development Professorship II in 2007–2010. His current research interests include the analysis, design, and real-time control of mechatronic systems, networked control systems, and nanoscale engineering and technology. He is the holder of three U.S. patents on precision positioning systems.

Dr. Kim is a Fellow of ASME and Member of Pi Tau Sigma. He was Technical Editor of IEEE/ASME Transactions on Mechatronics, *ASME Journal of Dynamic Systems, Measurement and Control, International Journal of Control, Automation, and Systems*, and *Asian Journal of Control*.